Laser heating of scanning probe tips for thermal near-field spectroscopy and imaging

Brian T. O'Callahan and Markus B. Raschke

Citation: APL Photonics **2**, 021301 (2017); doi: 10.1063/1.4972048
View online: http://dx.doi.org/10.1063/1.4972048
View Table of Contents: http://aip.scitation.org/toc/app/2/2
Published by the American Institute of Physics

Laser heating of scanning probe tips for thermal near-field spectroscopy and imaging

Brian T. O'Callahan and Markus B. Raschke[a]
Department of Physics, Department of Chemistry, and JILA, University of Colorado at Boulder, Boulder, Colorado 80309, USA

(Received 11 October 2016; accepted 29 November 2016; published online 27 December 2016)

Spectroscopy and microscopy of the thermal near-field yield valuable insight into the mechanisms of resonant near-field heat transfer and Casimir and Casimir-Polder forces, as well as providing nanoscale spatial resolution for infrared vibrational spectroscopy. A heated scanning probe tip brought close to a sample surface can excite and probe the thermal near-field. Typically, tip temperature control is provided by resistive heating of the tip cantilever. However, this requires specialized tips with limited temperature range and temporal response. By focusing laser radiation onto AFM cantilevers, we achieve heating up to ~1800 K, with millisecond thermal response time. We demonstrate application to thermal infrared near-field spectroscopy (TINS) by acquiring near-field spectra of the vibrational resonances of silicon carbide, hexagonal boron nitride, and polytetrafluoroethylene. We discuss the thermal response as a function of the incident excitation laser power and model the dominant cooling contributions. Our results provide a basis for laser heating as a viable approach for TINS, nanoscale thermal transport measurements, and thermal desorption nano-spectroscopy. [http://dx.doi.org/10.1063/1.4972048]

I. INTRODUCTION

Nanoscale thermal measurements based on scanning probe microscopy typically require independent control of tip and sample temperature. Tip temperature control has often been provided through Joule heating by flowing current through highly doped, conductive cantilever legs across a low-doped, resistive tip region.[1] Such electrically heated tips mounted at the end of cantilevers have been successfully used for chemical nano-identification based on melting point,[2] for nano-machining,[3] and to thermally excite a sample to perform thermal infrared near-field spectroscopy (TINS).[4,5]

In close proximity to a heated surface, a significantly enhanced electromagnetic density of states compared to the far-field limit may exist arising from non-propagating, high-wavevector mode contributions. The enhancement is strong in the presence of vibrational resonances, which can have sharp spectral peaks that can be used for chemical identification. Near-field spectroscopy using scattering-type scanning near-field optical microscopy (*s*-SNOM) of a thermally excited surface can reveal the unique spectral, spatial, and coherence properties of the resonantly enhanced thermal near-field. In a related scanning probe microscopy modality, nanofabricated tips with embedded thermocouples at their apex have been designed for measurements of enhanced thermal transport in the thermal near-field.[6]

However, the micron-scale precision needed to fabricate electrodes and doping variations in cantilevers is difficult. Joule-heated tips typically have larger apex radii of curvature limiting spatial resolution, require complex fabrication, and yield a low near-field optical signal as the electrodes

[a]Electronic address: markus.raschke@colorado.edu

often preclude metallic coating and limit the type of possible tip materials. Additionally, electrically heated tips are limited to maximum temperatures of up to ~900 K by "thermal runaway," whereby an increasing thermally excited carrier density reduces the resistance with increasing temperature and creates a positive feedback mechanism. This effect makes precise control of the temperature difficult. In addition, the heating is no longer localized to the tip as the cantilever also heats significantly.[7]

As an alternative, AFM probe heating through focused laser irradiation has been used to heat tips for thermal conductivity measurements,[8,9] for photothermal actuation of cantilevers,[10] and for nano-machining.[11] Here, we demonstrate laser heating and thermal control of simple cantilever tips to perform TINS. We characterize heating and cooling rates as well as tip temperatures. Using TINS, we perform spectroscopy on the vibrational resonances of hexagonal boron nitride (hBN), silicon carbide (SiC), and polytetrafluoroethylene (PTFE). Good agreement between theory and experiment is found with the vibrational frequencies of PTFE and the in-plane and out-of-plane phonon polariton (PhP) modes of hBN. The surface phonon polariton (SPhP) resonance of SiC is strongly red-shifted since it is highly sensitive to extrinsic perturbation.

II. EXPERIMENT

We use a continuous-wave laser (Verdi-G, Coherent, $\lambda = 532$ nm) for photothermal heating of Si cantilevers (Access-NC, AppNano) while operating in dynamic-mode AFM feedback. As shown in Fig. 1(a), the laser is fiber-coupled using a multimode fiber (core diameter $\phi = 62.5$ μm) into an overhead imaging arm and focused onto the backside of the cantilever by a microscope objective (NA = 0.3, f = 16 mm), which in turn allows for monitoring the $\phi \sim 10$ μm laser spot with a CCD imaging system. A long-pass filter blocks the scattered and reflected light from the AFM feedback laser beampath ($\lambda = 670$ nm) to prevent crosstalk with the AFM operation. The cantilevers are custom coated with platinum-iridium on the tip-side to enhance the thermal near-field but uncoated on the backside to allow efficient laser absorption. The heating is largely localized to the tip-end of the cantilever. The cantilever resonance frequency at $f \sim 300$ kHz shifts by 1%-2% at moderate temperatures, which is small enough to not disturb dynamic-mode feedback. Far-field tip emission spectra indicate that heating up to the melting point of Si can be achieved (~1800 K), with a correspondingly broad IR emission spectrum (Fig. 1(b)).

When the AFM tip is brought into contact with the sample, the sharp apex couples to the thermally excited near-field and scatters the evanescent field into detectable far-field radiation. The tip is kept stationary while the sample is raster scanned for spatial imaging. Tip-scattered light is collected with an off-axis parabolic mirror (f = 20.8 mm, NA = 0.48) and sent to a Michelson interferometer with

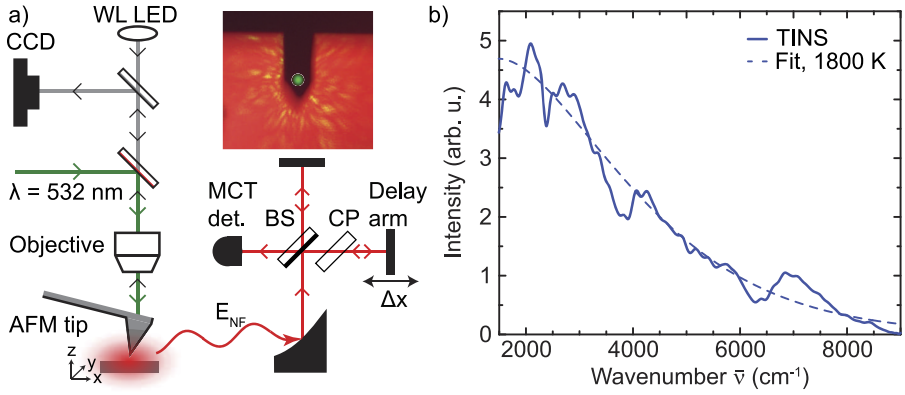

FIG. 1. Laser radiation ($\lambda = 532$ nm) is combined with white light from an LED with a dichroic beam splitter, and focused onto the backside of the cantilever with a microscope objective. A CCD camera allows imaging of the tip, the heating laser, and the sample surface. The inset image shows an overhead view of the tip cantilever, with depiction of heating laser spot. The sample is indirectly heated locally through conduction across the tip-sample gap. The evanescent thermal near-field is scattered by the apex of the tip into far-field radiation, collected by an off-axis parabolic mirror and detected interferometrically. (b) Far-field emission spectrum from the tip indicates heating to ~1800 K, with blackbody fit (dashed).

a beamsplitter (BS) and a compensation plate (CP) and detected with a mercury-cadmium-telluride (MCT) detector (J15D14, EG&G). We use either a BaF_2 beamsplitter (with a IR frequency cut-off at 900 cm^{-1}) or a KBr beam splitter (with transparency down to 500 cm^{-1}, however with slightly lower transmission) depending on the desired IR spectral region.

Lock-in demodulation of the optical signal at the tip-dither frequency (Ω) discriminates the near-field light from the far-field background.[12] With the near-surface spatial confinement of the thermal near-field, the low emissivity of the metal tip coating, and the localized heating generally confined to the tip shaft and its immediate surroundings, the far-field background is small and we find first harmonic demodulation sufficient for near-field extraction, in contrast to the use of higher harmonic demodulation as used in *s*-SNOM under external illumination. In conventional IR *s*-SNOM the illumination focal spot is much larger than the tip shaft, and interference from multiple reflections gives rise to a large and distance dependent background. Our finding is consistent with previous results of first-harmonic demodulation in TINS, showing ~50 nm spatial resolution for spectrally integrated studies.[4,5,13] Although higher order harmonics provide higher spatial resolution and improved background subtraction, they have generally weaker signal-to-noise ratios.[12] We perform Fourier transform infrared spectroscopy (FTIR) by scanning the delay arm controlled with a closed-loop delay stage (ANT95-50-L, Aerotech). A compact design (delay arm length ~12 cm) minimizes propagation losses and facilitates alignment.

The scattered signal reflects the thermal energy density $u_{\mathrm{den}}(\omega, z, T)$ at distance z from the sample surface at temperature T, which is given by the product of the electromagnetic local density of states $\rho(\omega, z)$ (EM-LDOS) and the mean energy of a thermally excited harmonic oscillator $\Theta(\omega, T) = \frac{\hbar\omega}{e^{\hbar\omega/k_BT}-1}$, $u_{\mathrm{den}}(\omega, z, T) = \rho(\omega, z)\Theta(\omega, T)$. The EM-LDOS is approximately given by $\rho(\omega, z) \simeq \frac{1}{4\pi^2\omega z^3}\frac{\mathrm{Im}(\varepsilon(\omega))}{|\varepsilon(\omega)+1|}$ in the quasistatic near-field limit, where $\varepsilon(\omega)$ is the sample dielectric function.[14]

III. RESULTS

Fig. 2 shows the IR emission characteristics of the laser-heated tips far from a surface. Spectra acquired with increasing laser power P (Fig. 2(a)) show an increase in overall intensity and a shift to higher frequencies with higher temperature. The spectra are fit to a blackbody spectral energy dependence $u(\bar{\nu}, T) = 2hc^2\bar{\nu}^3\frac{1}{e^{hc\bar{\nu}/k_BT}-1}$ multiplied by a power law $D(\bar{\nu}) \propto \bar{\nu}^{1.2}$ to incorporate the spectral dependence in MCT detectivity (dashed lines). This power law detectivity dependence was determined by far-field calibration using a blackbody emitter at a known temperature. With increasing laser intensity, we see an increase in temperature up to 610 K. The highest usable temperatures for near-field imaging and spectroscopy are limited by AFM feedback stability to a more moderate temperature range of 600-700 K. At higher temperatures the cantilever spring constant is reduced and its

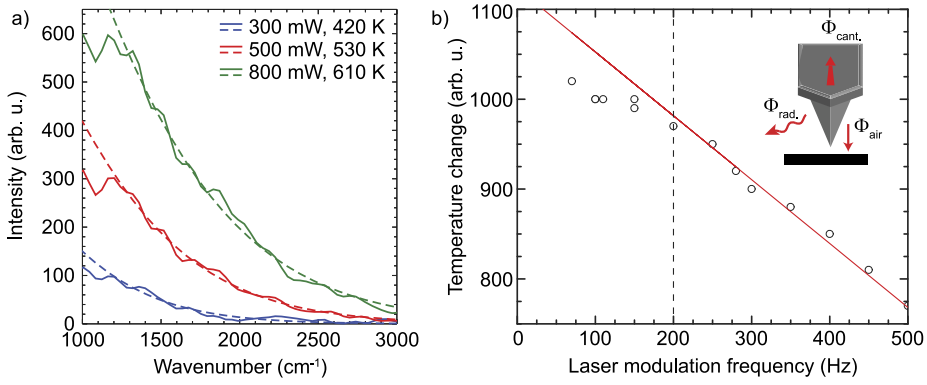

FIG. 2. (a) Far-field tip emission spectra as a function of laser heating power P. Spectra are fit to a blackbody model multiplied by a power law to correct for MCT detectivity. (b) Heating dynamics measured by modulating the heating laser power P = 450 mW and measuring the spectrally integrated infrared emission.

resonance frequency simultaneously red-shifts and broadens. Additionally, the resonance becomes less well-defined, possibly due to temperature inhomogeneities across the cantilever.

By using an optical chopper to periodically modulate the heating laser intensity (P = 450 mW) and measuring the spectrally integrated IR emission at the chopper frequency, we can estimate the cooling rate of the tip. When the laser is on, the tip heats up rapidly until an equilibrium is reached between the constant heating power and the cooling pathways (described below). When the laser is off, the temperature decreases exponentially and the emitted radiation intensity decays. For sufficiently long modulation times, the tip relaxes to ambient temperature and the temperature difference, and therefore the change in optical signal between heating cycles saturates. In Fig. 2(b) this saturation occurs below 200 Hz, indicating a cooling time of less than 5 ms.

Fig. 3(a) shows interferograms of tip-scattered IR light of a hBN/SiO_2 structure (hBN thickness = 200 nm) (blue), and with the tip far from the sample (red) as a reference measurement. The green curve is a fit to the long-lived oscillations away from zero path delay, which captures the resonant, temporally coherent contribution to the signal due to the PhP resonance of hBN. Fig. 3(b) shows the corresponding spectra from the interferograms in Fig. 3(a). The near-field spectrum of hBN shows peaked emission at the in-plane transverse-optical (TO) phonon mode frequency at $\bar{\nu}_{\parallel}^{\mathrm{TO}} = 1350\ \mathrm{cm}^{-1}$.

The blue curves in Figs. 3(c) and 3(d) show the interferogram and spectrum acquired on a hBN/Au structure (hBN thickness ~2 μm). In this case, the out-of-plane mode at $\nu_{\perp}^{\mathrm{TO}} = 780\ \mathrm{cm}^{-1}$ dominates the spectrum, while the in-plane mode is absent (discussed below). The spectral positions of the in-plane mode and the out-of-plane mode from Figs. 3(b) and 3(d) agree with the literature values.[15,16]

Fig. 4(a) shows the TINS interferogram of PTFE (blue), fit to the long-lived oscillations (green), and envelope of the exponential decay of the fit (purple). The near-field spectrum of PTFE shown in Fig. 4(b) shows peaks that closely match the $u_{\mathrm{den}}(\omega, z, T)$ calculated using dielectric values from the

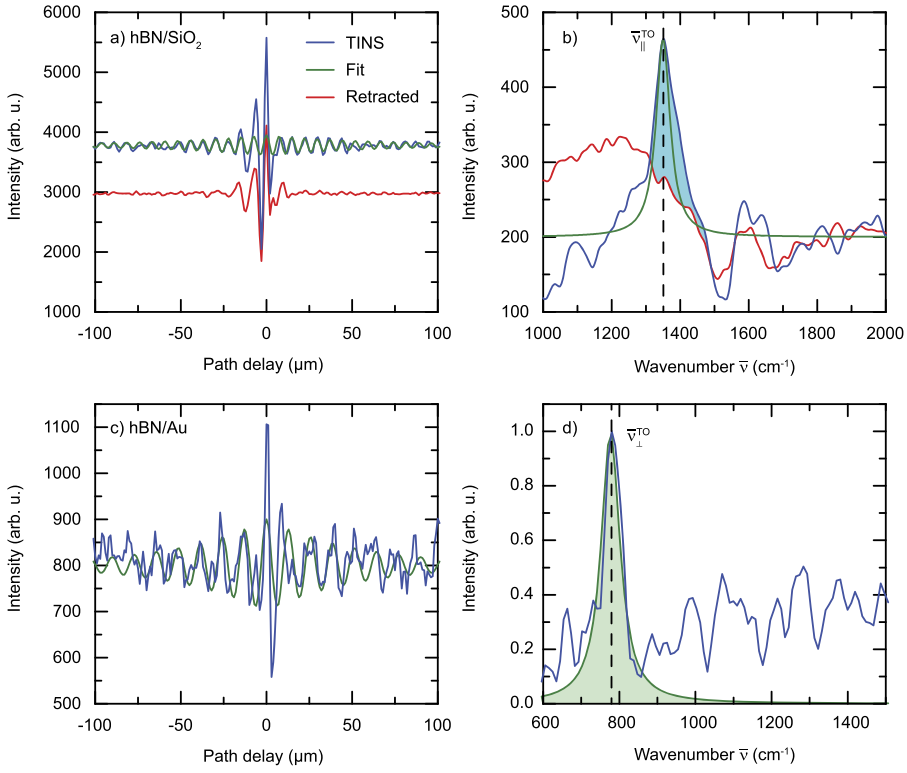

FIG. 3. (a) TINS interferogram and (b) spectrum of hBN on a SiO_2 substrate. Peaked thermal emission occurs at the in-plane phonon mode frequency $\bar{\nu}_{\parallel}^{\mathrm{TO}} = 1350\ \mathrm{cm}^{-1}$. Red curves are reference tip emission measurements acquired far from the sample surface. (c) Interferogram and (d) spectrum of hBN on a Au substrate are dominated by the out-of-plane phonon response at $\bar{\nu}_{\perp}^{\mathrm{TO}} \simeq 780\ \mathrm{cm}^{-1}$.

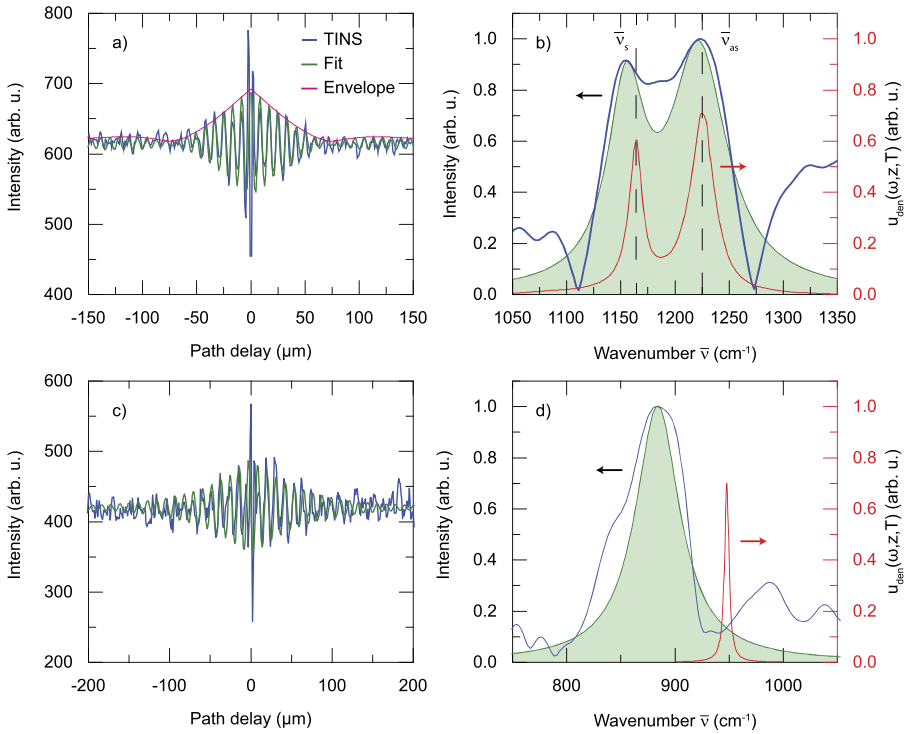

FIG. 4. (a) Interferogram and (b) spectrum of PTFE showing peaks at the symmetric and antisymmetric C-F vibrational mode frequencies. (c) Interferogram and (d) spectrum of SiC showing a strongly red-shifted response of the SPhP.

literature.[18] The peaks correspond to the symmetric $\bar{\nu}_s = 1158\ \mathrm{cm}^{-1}$ and the unresolved superposition of the two antisymmetric $\bar{\nu}_{as} = 1210$ and $1240\ \mathrm{cm}^{-1}$ C-F vibration modes.

The TINS spectrum of SiC shows a strong peak at $\sim 885\ \mathrm{cm}^{-1}$ (Figs. 4(c) and 4(d)). The red curve shows calculations of $u_{\mathrm{den}}(\omega, z, T)$ at temperature $T = 600$ K and distance $z = 50$ nm from the surface using literature values of the dielectric function, which peaks at $\omega = 948\ \mathrm{cm}^{-1}$, due to the surface phonon polariton of SiC.[17] The observed near-field peak is significantly red-shifted due to tip-sample coupling, as discussed below.

IV. DISCUSSION

The near-field spectrum of hBN/SiO_2 shows peaked emission at $\bar{\nu}_{\parallel}^{\mathrm{TO}} = 1350\ \mathrm{cm}^{-1}$, matching the in-plane phonon mode resonance frequency (Fig. 3(b)).[15,16] The out-of-plane mode response at $\nu_{\perp}^{\mathrm{TO}} = 780\ \mathrm{cm}^{-1}$ is not observed due to the use of a BaF_2 beam splitter with an IR bandwidth cut-off at $\sim 900\ \mathrm{cm}^{-1}$. In contrast, the near-field spectrum using a KBr beam splitter of hBN on a Au substrate shows a peaked signal at the out-of-plane phonon mode resonance frequency $\nu_{\perp}^{\mathrm{TO}} = 780\ \mathrm{cm}^{-1}$, while the in-plane mode is not observed. The absence of the in-plane phonon response may be due to screening from the Au substrate which reduces the in-plane mode strength while enhancing the out-of-plane phonon response.

In Fig. 4(b), the TINS peak positions of PTFE are not shifted compared to calculations of the energy density, since its localized vibrational modes are minimally sensitive to external perturbation by tip-sample coupling. In contrast, the TINS spectrum peak position of SiC is strongly red-shifted with respect to the peak frequency of $u_{\mathrm{den}}(\omega, z, T)$, due to tip-sample coupling or a change in dielectric environment due to the presence of the tip.[5,19] Phonon softening can contribute to a 6-7 cm^{-1} red-shift upon heating up to 550 K. However, the $\sim 60\ \mathrm{cm}^{-1}$ red-shift is larger than previously observed and cannot be adequately explained by conventional tip-sample coupling models or phonon softening.[20] Additionally, the effective medium model is not applicable to metallic tip materials with negative dielectric functions.[5] Instead, we attribute this large red-shift to stronger tip-sample coupling and

modification of the local field distribution due to the metallic tip. In contrast, the peak positions of hBN closely match the phonon mode frequencies, since it is not a truly surface confined polariton, and thus it is expected to be less susceptible to extrinsic perturbation.

The high laser powers necessary for significant heating are due to high thermal dissipation of the cantilevers, which can occur through several mechanisms. The heat flow through the cantilever ($\Phi_{cant} = -\frac{\kappa}{\Delta x} A \Delta T$) is roughly $3 \cdot 10^{-4}$ W/K, for our cantilever cross-section of $A \simeq 300\ \mu m^2$ and Si thermal conductivity of $\kappa_{Si} = 1.3$ (W/cm)/K. Radiated heat flow calculated with the Stefan-Boltzmann law is negligible ($\Phi_{rad} \sim 10^{-13}$ W). Heat conduction from the cantilever through air is more difficult to quantify and depends on numerous parameters such as tip height; however it has been estimated to be on the order of $\Phi_{air} \sim 10^{-5}$ W/K.[21] These thermal dissipation pathways determine the temperature dynamics shown in Fig. 2(b) which may prove critical for frequency-resolved thermal measurements,[22] thermal actuation of cantilevers,[10] improving signal-to-noise by reducing $1/f$ measurement noise,[23] or for high-speed fabrication techniques using laser-heated tips.[24,25] Careful control of these thermal pathways could allow optimization of the thermal time constant for the desired implementation.

In summary, we have demonstrated laser tip heating for TINS with temperature range up to the melting point of Si and providing near-field spectra across a wide range of samples. Further improvements to increase TINS sensitivity include utilizing higher-sensitivity photodetectors, and modifying cantilevers to improve AFM stability at higher temperatures. Heating through photoexcitation can provide a platform for nanoscale heat transfer experiments by controlling input heat while monitoring tip temperature. These heat transfer and thermal conductivity measurements can be performed simultaneously with near-field spectroscopy to identify the underlying optical processes. Also, this technique may replace electrically heated tips for thermal-desorption-based chemical analysis using mass spectroscopy.[26] The high temperatures achievable through photothermal excitation also allow tip-based nano-fabrication of a wider range of materials with higher melting temperatures than previously accessible. Due to the simplicity of the approach, cantilever materials are not limited to doped-Si and have more design versatility to improve heating dynamics and localization, extending the application space of tip-based thermal measurements and nano-machining.

ACKNOWLEDGMENTS

We gratefully acknowledge valuable support from Bernd Metzger, and Jun Yan. Funding was provided by the U.S. Department of Energy, Office of Basic Sciences, Division of Material Sciences and Engineering, under Award No. DE-SC0008807.

[1] B. A. Nelson and W. P. King, in *Applied Scanning Probe Methods IV*, NanoScience and Technology, edited by B. Bhushan and H. Fuchs (Springer Berlin Heidelberg, 2006), pp. 251–275, ISBN: 978-3-540-26912-0.
[2] B. Nelson and W. King, Sens. Actuators, A **140**, 51 (2007).
[3] A. Knoll, P. Bächtold, J. Bonan, G. Cherubini, M. Despont, U. Drechsler, U. Dürig, B. Gotsmann, W. Häberle, C. Hagleitner *et al.*, Microelectron. Eng. **83**, 1692 (2006).
[4] A. C. Jones and M. B. Raschke, Nano Lett. **12**, 1475 (2012).
[5] B. T. O'Callahan, W. E. Lewis, A. C. Jones, and M. B. Raschke, Phys. Rev. B **89**, 245446 (2014).
[6] K. Kim, B. Song, V. Fernández-Hurtado, W. Lee, W. Jeong, L. Cui, D. Thompson, J. Feist, M. T. H. Reid, F. J. García-Vidal *et al.*, Nature **528**, 387 (2015).
[7] B. W. Chui, M. Asheghi, Y. S. Ju, K. E. Goodson, T. W. Kenny, and H. J. Mamin, Microscale Thermophys. Eng. **3**, 217 (1999).
[8] M. Nonnenmacher and H. K. Wickramasinghe, Appl. Phys. Lett. **61**, 168 (1992).
[9] D. Sarid, B. McCarthy, and R. Grover, Rev. Sci. Instrum. **77**, 023703 (2006).
[10] H. Adam, S. Rode, M. Schreiber, K. Kobayashi, H. Yamada, and A. Kühnle, Rev. Sci. Instrum. **85**, 023703 (2014).
[11] A. Chimmalgi, T. Y. Choi, C. P. Grigoropoulos, and K. Komvopoulos, Appl. Phys. Lett. **82**, 1146 (2003).
[12] B. Knoll and F. Keilmann, Opt. Commun. **182**, 321 (2000).
[13] F. Peragut, J.-B. Brubach, P. Roy, and Y. De Wilde, Appl. Phys. Lett. **104**, 251118 (2014).
[14] K. Joulain, R. Carminati, J.-P. Mulet, and J.-J. Greffet, Phys. Rev. B **68**, 245405 (2003).
[15] Y. Cai, L. Zhang, Q. Zeng, L. Cheng, and Y. Xu, Solid State Commun. **141**, 262 (2007).
[16] J. D. Caldwell, A. V. Kretinin, Y. Chen, V. Giannini, M. M. Fogler, Y. Francescato, C. T. Ellis, J. G. Tischler, C. R. Woods, A. J. Giles *et al.*, Nat. Commun. **5**, 5221 (2014).
[17] E. Palik, *Handbook of Optical Constants of Solids, Five-Volume Set: Handbook of Thermo-Optic Coefficients of Optical Materials with Applications* (Elsevier Science, 1997), ISBN: 9780080523750, URL https://books.google.com/books?id=FeeNeEzQ3GMC.
[18] G. Masetti, F. Cabassi, G. Morelli, and G. Zerbi, Macromolecules **6**, 700 (1973).

[19] A. Babuty, K. Joulain, P.-O. Chapuis, J.-J. Greffet, and Y. De Wilde, Phys. Rev. Lett. **110**, 146103 (2013).
[20] A. Cvitkovic, N. Ocelic, and R. Hillenbrand, Opt. Express **15**, 8550 (2007).
[21] W. P. King, B. Bhatia, J. R. Felts, H. J. Kim, B. Kwon, B. Lee, S. Somnath, and M. Rosenberger, Ann. Rev. Heat Transfer **16**, 287 (2013).
[22] O. Kwon, L. Shi, and A. Majumdar, J. Heat Transfer **125**, 156 (2003).
[23] S. Lefévre and S. Volz, Rev. Sci. Instrum. **76**, 033701 (2005).
[24] H. J. Mamin, Appl. Phys. Lett. **69**, 433 (1996).
[25] B. W. Chui, T. D. Stowe, Y. S. Ju, K. E. Goodson, T. W. Kenny, H. J. Mamin, B. D. Terris, R. P. Ried, and D. Rugar, J. Microelectromech. Syst. **7**, 69 (1998).
[26] O. S. Ovchinnikova, K. Kjoller, G. B. Hurst, D. A. Pelletier, and G. J. V. Berkel, Anal. Chem. **86**, 1083 (2014).